

Inclusive fluxes of secondary air-shower particles

Hariom Sogarwal and Prashant Shukla

Nuclear Physics Division, Bhabha Atomic Research Centre, Mumbai 400085, India
Homi Bhabha National Institute, Anushakti Nagar, Mumbai 400094, India

E-mail: sogarwalhariom@gmail.com, pshuklabarc@gmail.com

Abstract. The particle showers produced in the atmosphere due to the interactions of primary cosmic particles require a thorough understanding in the backdrop of searches for rare interactions. In this work, we made a comprehensive study of air shower simulations using various combinations of hadronic models and particle transport code of the CORSIKA package. The primary proton and helium distributions are taken as power law which are scaled to match the measured flux in balloon and satellite-based experiments at the top of atmosphere. The shower simulation includes production, transport and decays of secondaries up to the ground level. In this study, we focus on the bulk of the spectra and particles which is computationally intensive and hence parallel processing of events is done on computer cluster. We provide a way to normalize the simulation results to be compared with the ground-based measurements namely, single and multiple muon yields and their charge ratios as a function of zenith angle and momentum. This provides a basis for comparisons among the six model combinations used in this study and the differences are outlined. Most of the hadronic models in CORSIKA produce the bulk ground based measurements fairly well. We use one of the best model combinations to quantitatively predict the absolute and relative yields of various particles at ground level as well as their correlations with primaries and with each other. The leptonic ratios are obtained as a function of energy and zenith angle which are important inputs for the neutrino oscillation physics.

Contents

1	Introduction	1
2	Parameterizations of muon distributions	3
3	CORSIKA simulation inputs	4
4	Results & discussions	5
4.1	Muon observables	6
4.2	Correlations of muons and primary particles	9
4.3	Flux and ratios of various particles	11
5	Conclusions	12

1 Introduction

The cosmic rays consisting of high energy charged particles continuously bombard the Earth from all directions and have remained one of the most interesting and active areas of research [1]. The particle showers produced in the atmosphere due to the interactions of these primary cosmic particles have provided a natural laboratory of physics of standard and beyond standard models which led to many discoveries. Accurate knowledge of both the primary as well as secondary particles is an important prerequisite for search of rare interactions. The primary cosmic rays consist of protons (90%), helium nuclei (9%) and other heavy nuclei (1%) which have been produced and accelerated in astrophysical processes to high energies as large as 10^8 TeV. Upon entering the atmosphere, the primary cosmic particles interact with the nuclei of oxygen and nitrogen gases roughly 12 km above Sea level. These interactions lead to the production of shower of hadrons, mainly pions and kaons with a small percentage of heavier particles which move downwards while losing energy and decaying. These particles introduce cosmogenic signal and background for the measurement of neutrino oscillation physics and hence their study is very useful to precisely understand the mass difference of the neutrinos in the 2-3 sector and the mass hierarchy. Although neutrinos are the most abundant shower particles at the Earth surface, muons are the most abundant charged particles and are responsible for half of the terrestrial radiation dose taken by a body on Earth. Measurements of muon distributions at ground is an active field and the improved theoretical understanding and detection technologies are providing more insights in the particle production in showers [2, 3]. LHC is working on a dedicated experiment of proton-oxygen collisions to understand the air shower physics. This dedicated LHC run will help in tuning of various hadronic interaction parameters used in the cosmic ray packages for better understanding of the air shower produced in the atmosphere and spectra of various particles at ground level [4].

The shower simulation codes employ hadronic interaction models which have energy dependent hadronic cross-section calculations as the main body of the simulation. CORSIKA is a Monte Carlo program for detailed simulation of air showers initiated by high-energy primary cosmic particles such as protons [5] using various hadronic interaction models which can be selected in the CORSIKA options (version 7.7100) [6]. For the hadronic interactions at high energies, the most popular models are QGSJET and SIBYLL. QGSJET [7–9] (Quark

Gluon String model with JETs) describes high-energy hadronic interactions using the quasi-eikonal pomeron parameterization for the elastic hadron-nucleon scattering amplitude. The hadronization process is treated in the quark gluon string model. The more improved version is QGSJET-II-04 [10, 11] which includes pomeron loop and the cross-sections are tuned to LHC data. SIBYLL [12–16] is a program developed to simulate hadronic interactions at extremely high energies based on the QCD mini-jet model. SIBYLL also activates the inelastic hadronic interaction cross-sections at higher energies which are based on QCD calculations. We use SIBYLL 2.3c version [16].

For low-energy (below 100 GeV) interactions, the popular packages are GHEISHA, UrQMD and FLUKA. GHEISHA (Gamma Hadron Electron Interaction SHower code) is a model which describes hadronic collisions up to some 100 GeV in many experiments. A detailed description of the physics processes covered by GHEISHA may be found in Ref. [17]. UrQMD (Ultra-relativistic Quantum Molecular Dynamics) is another package designed to treat low-energy hadron-nucleus interactions. A detailed description of this model may be found in Ref. [18, 19]. UrQMD 1.3 is used in CORSIKA to perform the elastic and inelastic interactions of hadrons below 80 GeV in air. FLUKA (FLUctuating KAscade) [20, 21] is a package of routines which transport energetic particles through matter by the monte carlo method. In combination with CORSIKA, only the low-energy hadronic interaction part is used which calculates the inelastic hadron cross-sections with the components of air and produce secondary particles including many details of the de-excitation of the target nucleus. CORSIKA is also used for generating showers for small local arrays [22]. There are also plans concerning the design and development for the new generation of CORSIKA for various scientific applications making an efficient use of computational resources [23].

CORSIKA is widely used for generating muons for detector simulations [24, 25]. There have been several studies to compare and validate different CORSIKA models with experimental data. In one of the initial studies [26], muon and neutrino flux ratios were obtained using various models of CORSIKA and comparison was made with experimental data and other theory models. The work in Ref. [27] used CORSIKA to obtain the muon momentum distributions at ground and at an altitude using VENUS and two low energy models GHEISHA and UrQMD which are compared with the measurements. Recently, work in Ref. [28] used four high energy models of hadronic interactions in CORSIKA to compare the distributions of different particles. The study outlines the differences between different models. The work in Refs. [29, 30] used CORSIKA to study the variations of shower angle distribution as a function of atmospheric depth from tens of TeV to PeV energies of protons.

There have been few recent studies of muon observables obtained with CORSIKA. The CORSIKA is used to study the dependence of the power index of angular distribution of muons on the energy and atmospheric depth using the QGSJET and GHEISHA models [31]. Bahmanabadi [32] measured the muon charge ratio in the low energy range and made a comparison with two low energy models (GHEISHA and UrQMD) in CORSIKA. Bahmanabadi and Fazlalizadeh [33] studied the east-west asymmetry as well as the muon charge ratio sensitivity to the low-energy GHEISHA and UrQMD in combination with the high energy QGSJET-II model. In Ref. [34], the momentum and angle distributions of muons obtained using CORSIKA are compared with the analytical formulae.

Many of the studies in the literature focussed on the hadronic models for very high-energy showers. Also many studies concentrated on the ratios of the particles rather than absolute yields. We planned our work to make a comprehensive study of air shower simulations using different combinations of low and high energy models in CORSIKA. In this study,

we focus on the bulk of the particles at ground level and obtain the absolute yields using normalized simulation results. We have used data for muon distributions namely, zenith angle distribution, momentum distributions (at 0° and 75°) and charge ratios to compare with six model combinations. The predictions are made for multiplicity and East-west asymmetry for muons for all model combinations. The leptonic distributions and ratios form an important input for neutrino oscillation studies.

Contribution in the different muon observables coming from different energy as well as zenith angle intervals of primary protons and heliums is obtained to correlate the ground based measurements with the initial particle direction and energy. We predict the zenith angle and momentum distributions of all other particles and their ratios which could be measurable at ground in addition to muons. The distributions of other hadronic and leptonic particles are obtained. Distributions of muons and neutrinos as a function of θ and ϕ is presented to quantify East-west asymmetry.

We perform CORSIKA simulation using various hadronic interaction models and obtain various distributions of particles at the ground. The low-energy hadronic interaction models used in this work are GHEISHA, UrQMD and FLUKA, whereas the high-energy interaction models are QGSJET, QGSJET-II and SIBYLL. The initial cosmic proton and helium distributions have been taken as power law which are matched with experimental data from balloon and satellite-based measurements. The muon distributions obtained are then compared with the experimental data measured at the ground level and with some of the recent parametrizations. In view of a dedicated run of proton oxygen collisions planned at LHC, such study becomes more important and timely.

2 Parameterizations of muon distributions

In this section, we describe the parametrizations which are used to compare with the CORSIKA simulations. The energy distribution of primary cosmic rays follows power law E^{-n} . The pion and the muon distributions also follow the same power law which is modified in the low-energy region [35] as

$$I(E) = I_o N (E_o + E)^{-n} \left(1 + \frac{E}{\epsilon}\right)^{-1}. \quad (2.1)$$

Here, $N = (n - 1) (E_o + E_c)^{(n-1)}$ is the normalization in which E_c ($= 0.5$ GeV) is the cut-off value of the data while E_o and ϵ are parameters. The zenith angle distribution of energy integrated flux in terms of $I_o = \Phi(\theta = 0)$ is obtained as

$$\Phi(\theta) = I_o D(\theta)^{n-1}, \quad (2.2)$$

where $D(\theta)$ is the ratio of pathlength of a muon from inclined direction to that of a muon from the vertical direction and is given by [35]

$$D(\theta) = \sqrt{\frac{R^2}{d^2} \cos^2 \theta + 2 \frac{R}{d} + 1} - \frac{R}{d} \cos \theta. \quad (2.3)$$

Here, d , R and θ are the vertical depth, radius of the Earth and the zenith angle respectively. For the case when the Earth is assumed to be flat, $D(\theta) = 1/\cos \theta$, the Eq. 2.2 leads to

$$\Phi(\theta) = I_o \cos^{n-1} \theta. \quad (2.4)$$

With $n \simeq 3$, this gives the usual $\cos^2 \theta$ distribution which is empirically known to describe zenith angle distribution. The values of the parameters for muon energy distributions corresponding to Eq. 2.1 are listed in the Table 1 [35]. Table 2 lists the values of parameters of muon zenith angle distribution corresponding to Eqs. 2.2 and 2.4 [35]. Table 3 lists the values of parameters of proton and helium energy distributions corresponding to Eqs. 2.1 which have been obtained in the present work.

Table 1. Parameters of Eq. 2.1 for muon energy distributions [35].

	I_o ($\text{m}^{-2}\text{s}^{-1}\text{sr}^{-1}$)	n	E_o (GeV)	$1/\epsilon$ (GeV) $^{-1}$
μ at 0° Sea level ($E > 0.5$ GeV)	70.7 ± 0.2	3.01 ± 0.01	4.29 ± 0.04	$1/854$
μ at 75° Sea level ($E > 1.0$ GeV)	65.2 ± 1.5	3.00 ± 0.02	23.78 ± 0.30	$1/2000$

Table 2. Parameters for zenith angle distribution functions of muons [35].

Function	I_o	n	R/d
$\Phi(\theta) = I_o D(\theta)^{n-1}$	88.0 ± 2.4	3.09 ± 0.03	174 ± 12
$\Phi(\theta) = I_o \cos^{n-1} \theta$	85.6 ± 2.4	3.01 ± 0.03	-

Table 3. Parameters of Eq. 2.1 for proton and helium energy distributions.

	$I_o N$	n	E_o (GeV)	$1/\epsilon$ (GeV) $^{-1}$	χ^2/NDF
Proton ($E > 1$ GeV)	16200 ± 513	2.760 ± 0.032	0.52 ± 0.11	0.0	50.19
Helium ($E > 1$ GeV)	759 ± 292	2.703 ± 0.002	0.31 ± 0.55	0.0	34.57

Gaisser had given analytical formula [36] for muon energy distribution assuming flat Earth and which is valid for high-energy $E_\mu > 100/\cos \theta$ GeV, is given by

$$\frac{dN_\mu}{dE \cdot d\Omega} \approx 1400 E_\mu^{-2.7} / (\text{m}^2 \text{s GeV sr}) \left(\frac{1}{1 + \frac{1.1 E \cos \theta}{\epsilon_\pi}} + \frac{0.054}{1 + \frac{1.1 E \cos \theta}{\epsilon_\kappa}} \right),$$

where the two terms in the bracket give the contributions of pions and kaons in terms of the two parameters $\epsilon_\pi \approx 115$ GeV and $\epsilon_\kappa \approx 850$ GeV.

3 CORSIKA simulation inputs

In our simulations, the atmospheric model was chosen as the Central European atmosphere for October month out of the available atmospheric models in the CORSIKA simulation. The

conditions are taken as central Europe which are also a close approximation to conditions at Tsukuba. The horizontal component (towards the North) and vertical component (downwards) of the Earth's magnetic field are taken as $30.07 \mu\text{T}$ and $35.32 \mu\text{T}$ respectively. The observation level is a sphere following the Earth's curvature at an altitude of 30 m.

The primary proton/helium energy distribution is chosen as the power law of the form

$$I = A E^{-2.7}. \quad (3.1)$$

The energy is generated in the range between 10 GeV and 5×10^5 GeV in our simulations. The simulation process is computationally intensive hence parallel processing of events at computer cluster has been performed. The primary particle is generated in nine intervals of energy given by [10, 50] GeV, [50, 10^2] GeV, [10^2 , 5×10^2] GeV, [5×10^2 , 10^3] GeV, [10^3 , 5×10^3] GeV, [5×10^3 , 10^4] GeV, [10^4 , 5×10^4] GeV, [5×10^4 , 10^5] GeV and [10^5 , 5×10^5] GeV. In each energy interval, 100000 events are generated except in the last interval in which 1000 events are generated.

The spectrum in each energy range is weighted by the factor f given as

$$f = \frac{E_1^{-1.7} - E_2^{-1.7}}{E_3^{-1.7} - E_4^{-1.7}}, \quad (3.2)$$

where $E_1 = 10$ GeV, $E_2 = 50$ GeV and E_3, E_4 are the lower and upper bound of a given energy interval. With this method, then we obtain the equivalent number of proton showers generated over the whole distribution in the energy range 10 - 5×10^5 GeV as "106,933".

The default primary intensity distribution of protons and heliums with the zenith angle θ in CORSIKA goes as

$$I(\theta) \sim \sin \theta. \quad (3.3)$$

The sine term respects the solid angle element of the sky. The ϕ distribution is taken as uniform between $-\pi$ to π .

Figure 1(a) shows the proton flux as a function of momentum falling at the top of the atmosphere as measured by balloon and satellite-based experiments [37–42] along with the proton spectrum used in the simulation and the parameterization given by Eq. 2.1. Figure 1(b) shows the helium flux as a function of momentum per nucleon falling at the top of the atmosphere as measured by balloon and satellite-based experiments [37, 38, 40–43] along with the initial helium spectrum used in the simulation and the parameterization given by Eq. 2.1. The momentum distributions of initial protons and heliums used in the simulation are represented here by histograms having logarithmic bins. It is observed that the momentum distribution of the primary particles roughly follow power law ($p^{-2.7}$) in the energy range from 10 GeV/ c to 5×10^5 GeV/ c considered in the present work. The primary proton and helium spectra are matched to the measured spectrum and scale factors are obtained which are used to obtain normalization for all the spectra obtained by protons and heliums in CORSIKA. The normalized spectra obtained from protons and heliums are then added.

4 Results & discussions

In CORSIKA, among low energy models, we choose GHEISHA, UrQMD and FLUKA and among high energy models we choose QGSJET, QGSJET-II and SIBYLL. Both QGSJET and QGSJET-II are the hadronic interactions models for the high-energies interactions and

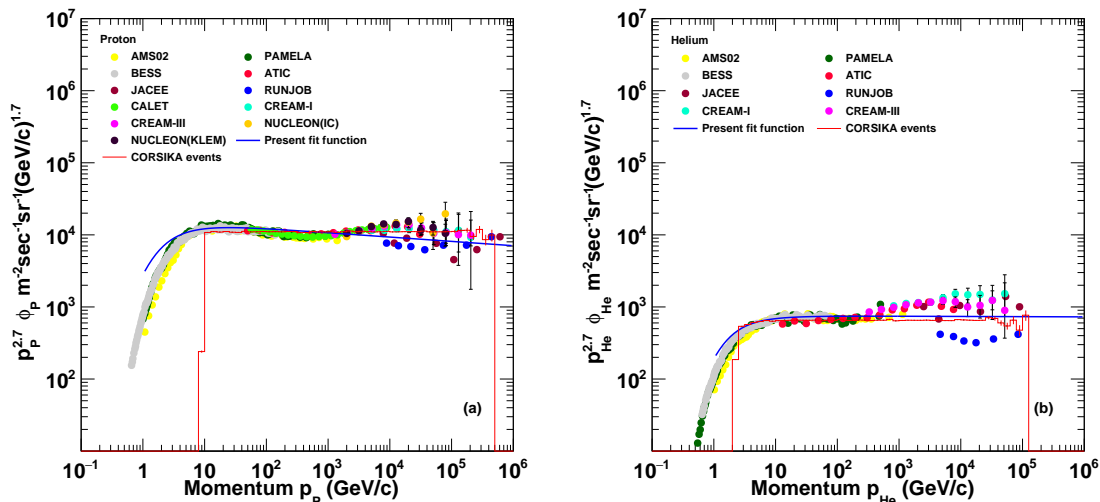


Figure 1. (a) The proton flux as a function of momentum falling at the top of the atmosphere as measured by balloon and satellite-based experiments [37–42] along with the initial proton spectrum used in the simulation and the parameterization given by Eq. 2.1. (b) The helium flux as a function of momentum per nucleon falling at the top of the atmosphere as measured by balloon and satellite-based experiments [37, 38, 40–43] along with the initial helium spectrum used in the simulation and the parameterization given by Eq. 2.1.

QGSJET-II is the upgraded form of QGSJET. Our interest was to see their similarity and differences in the bulk of the particles spectrum at ground level. In earlier investigations of cosmic muons at LEP, the hadronic interactions were simulated using QGSJET 01. Besides the treatment of nonlinear effects, another notable contrast between the previous model and QGSJET II-03/04 is the steeper lateral distribution which gives the greater penetration in the Earth’s atmosphere and higher value of shower maximum, X_{\max} , in the later versions.

We make six model combinations as follows:

1. [A] GHEISHA & QGSJET
2. [B] UrQMD & QGSJET
3. [C] UrQMD & QGSJET-II
4. [D] GHEISHA & SIBYLL
5. [E] UrQMD & SIBYLL
6. [F] FLUKA & SIBYLL

We describe our studies in the following three subsections.

4.1 Muon observables

Here, we describe the results for the studies done on the muon observables which are either measured or can be easily measured at ground level detectors. Same normalization factor is going for secondary fluxes which is obtained by matching the input primary momentum

distribution with the experimental data at the top of atmosphere. Thus, simply the flux at ground is obtained in the same unit as the measured flux at the top. The zenith angle and momentum spectra of muons obtained by CORSIKA are scaled by $1/\sin\theta$ to remove the effect of solid angle dependence on zenith angle θ . Other than that we have only angle bin correction in which sampling is done given by the factor $F = (\pi/2)/\Delta\theta$, where $\Delta\theta$ is the θ bin size. Here, $\pi/2$ is the total zenith angle coverage. We calculate the χ^2/n (per degree of freedom) for each of the spectra given by

$$\chi^2/n = \frac{1}{n} \sum_{i=1}^n \left(\frac{\phi_i^{\text{data}} - \phi_i^{\text{corsika}}}{\sqrt{(\Delta\phi_i^{\text{data}})^2 + (\Delta\phi_i^{\text{corsika}})^2}} \right)^2. \quad (4.1)$$

Here, $\phi_i^{\text{corsika}} \pm \Delta\phi_i^{\text{corsika}}$ is the value of the flux with statistical error in CORSIKA and $\phi_i^{\text{data}} \pm \Delta\phi_i^{\text{data}}$ is the same in data for bin i with total number of bins n . Wherever experimental data was not available for a bin, the parametrization function was used to interpolate between data points.

Knowledge of muon zenith angle distributions, momentum distributions at zero and higher angles are important for the calibrations of the detectors at underground labs which are dedicated to measure the rare physics events. The shape and extent of these distributions depend on the material thickness. Thus they are useful in the estimations of depth of underground labs and detector material budget for such experiments. Figure 2 shows the zenith angle distributions calculated with CORSIKA using various model combinations for muon momentum $p > 0.5$ GeV/ c along with the data measured by various experiments. The parameterization given by Eq. 2.2 is also shown [35]. The data are taken from the collection of Ref. [46] with the original references [47–50]. The different datasets have different muon energy thresholds and we take the normalized data from the review [46]. Various models have differences in the hadronic multiplicity production and energy sharing among particles produced which actually affects the muon multiplicities at ground level and shower extent in the atmosphere. For example, in the QGSJET-II model, the shower depth X_{max} is larger than that in QGSJET and hence gives more contribution in the lower zenith angles.

Figure 3 shows the momentum distribution of vertical atmospheric muons at the ground level calculated by CORSIKA using different hadronic interaction model combinations for $p > 0.5$ GeV/ c along with the experimental data [51, 52]. The parametrizations given by Eq.2.1 and Eq.2.5 are also shown. The plots in Figure 3 are obtained by integrating all muons falling between 0 to 10 degrees and are scaled by $F = (\pi/2)/\Delta\theta$, where $\Delta\theta = 10^\circ$. All model combinations give a good description of experimental data although all underestimate the muon flux in the very low energy region. The parametrization by Eq.2.1 gives a good description of the data.

Figure 4 shows the momentum distribution of atmospheric muons at 75° zenith angle at the ground level calculated by CORSIKA using the different hadronic interaction model combinations for $p > 0.5$ GeV/ c along with the experimental data [53]. The parametrizations given by Eq. 2.1 and Eq. 2.5 are also shown. The plots in Figure 4 are obtained by integrating all muons falling between 71 to 81.8 degrees and are scaled by $F = (\pi/2)/\Delta\theta$, where $\Delta\theta = 10.8^\circ$. All model combinations give a good description of experimental data although all underestimate the muon flux in the very low energy region. Models [D], [E] and [F] give a good description of the data. The parametrization by Eq. 2.1 gives a good description of the data.

The χ^2/n calculated (with Eq. 4.1) for all the models corresponding to Figures 2, 3 and 4 are given in Table 4. For χ^2/n calculations the muon cosine zenith angle range from 0.1 to 1 and the momentum range from 1 GeV/c to 5 TeV/c are included. Wherever experimental data was not available, the parametrization function was used to interpolate between data points. All the model combinations produce the shape of zenith angle distribution given by $\cos^2 \theta$ and models [A], [C] and [D] give good descriptions of the data. The mismatch at higher angles is due to flat Earth approximation used in CORSIKA and this mismatch exists for all model combinations. The parametrization given by Eq. 2.2 produces the shape of the distribution at all angles.

Table 4. Calculated χ^2/n for the cosine of zenith angle distribution and momentum distributions at 0° and 75° from CORSIKA models.

Model Combination	χ^2/n		
	for θ distribution	for momentum at 0°	for momentum at 75°
[A] GHEISHA & QGSJET	4.28	1.62	8.83
[B] UrQMD & QGSJET	6.52	1.23	7.46
[C] UrQMD & QGSJET-II	4.24	2.39	6.63
[D] GHEISHA & SIBYLL	2.79	1.80	3.52
[E] UrQMD & SIBYLL	5.69	1.69	1.09
[F] FLUKA & SIBYLL	5.20	1.43	1.47

The integrated muon fluxes for all the model combinations calculated from zenith angle distribution and from momentum distributions at 0° and 75° are given in the Table 5. The integrals obtained from theta distribution are multiplied with the $2\pi \cdot (\pi/2)$ to cover the whole solid angle. We find that the integrated muon flux given by all interaction models reasonably match with each other except for combination [C] UrQMD & QGSJET-II which is higher in all 3 cases. The effect of deeper shower maximum in case of QGSJET-II with respect to QGSJET can be easily seen in the muon zenith angle and momentum distributions and in the integrated values in the Table 5 [B] and [C] models.

Table 5. Integrated muon flux for different models at ground level for muon momentum $p > 0.5$ GeV/c.

Model Combination	Integrated muon flux		
	for θ distribution ($\text{m}^{-2}\text{sec}^{-1}$)	for momentum at 0° ($\text{m}^{-2}\text{sec}^{-1}\text{sr}^{-1}$)	for momentum at 75° ($\text{m}^{-2}\text{sec}^{-1}\text{sr}^{-1}$)
[A] GHEISHA & QGSJET	184.80	75.55	1.32
[B] UrQMD & QGSJET	191.49	73.20	1.28
[C] UrQMD & QGSJET-II	197.59	80.38	1.35
[D] GHEISHA & SIBYLL	183.29	74.97	1.33
[E] UrQMD & SIBYLL	190.00	73.19	1.25
[F] FLUKA & SIBYLL	189.85	80.74	1.26

Figure 5 shows the charge ratio μ^+/μ^- as a function of the momentum of atmospheric muons at the ground level calculated by CORSIKA using the different hadronic interaction model combinations along with the experimental data collection [3]. The original references of experimental data are BESS [51], CMS [54], MINOS [55], OPERA [56] and L3+C [57]. The

jump in the momentum around 20 GeV/ c is due to the transition between low and high energy models. Muon charge ratio is more than 1 because there are more π^+ than π^- produced in the shower due to the positive charge of the proton. In the higher momentum side, the increase in the charge ratio is due to the associated production of strange particles, neutral lambda and positively charged kaons which decay to positive pions and muons. Muon charge ratio as a function of momentum is very important to know the underlying physics of hadronic interactions in the atmosphere and production of various hadrons in different fraction and energy. The combination of models [F] FLUKA & SIBYLL gives the best results for the muon charge ratio in the given momentum range as compared to other model combinations.

Figure 6 shows the charge ratio μ^+/μ^- as a function of zenith angle of atmospheric muons for momentum $p > 0.5$ GeV/ c at the ground level calculated by CORSIKA using different hadronic interaction model combinations, [A] GHEISHA & QGSJET, [B] UrQMD & QGSJET, [C] UrQMD & QGSJET-II, [D] GHEISHA & SIBYLL, [E] UrQMD & SIBYLL, [F] FLUKA & SIBYLL. Integer numbers are added to models other than [A] as shown to separate the results. Most of the models give charge ratio around 1.2 and which remains almost flat as a function of zenith angle but slightly increases towards higher angles (60-80 degrees) for the models [A], [C], [D] and [E]. The results can be compared with measured data. As the shower traverses larger path at higher zenith angles the number of hadronic interactions and production of particles will be different which can contribute differently in the muon charge ratio. The ratio increases towards higher zenith angle as the contribution from higher energy particles which could cross the larger length. It will be interesting to have muon charge measurements as a function of zenith angle.

Figure 7 shows the multiplicity of muons in a shower calculated for muon momentum $p > 0.5$ GeV/ c using (a) [F] FLUKA & SIBYLL model of CORSIKA. (b) Shows the multiplicity ratios of model combinations ([A] GHEISHA & QGSJET, [B] UrQMD & QGSJET, [C] UrQMD & QGSJET-II, [D] GHEISHA & SIBYLL and [E] UrQMD & SIBYLL) with respect to [F] FLUKA & SIBYLL model. An integer number is added to each model result as shown in figure. It can be seen from the ratios that all models give similar shape of multiplicity distributions. High energy model in case of [D], [E] and [F] model combination is SIBYLL. Therefore, the multiplicity distribution is nearly same in all 3 models and other model combinations [A], [B] and [C] show some disagreement. At high energies or for heavier nuclei, the multiplicity might show more disagreements. Multiplicity distributions shapes are important to get the extent of air shower at the ground level which will be useful to understand the multiple muon events in the large size detectors from each shower.

4.2 Correlations of muons and primary particles

Contributions in the different muon observables coming from different energy as well as zenith angle intervals of primary protons and heliums are obtained. The primary particles and their energy dependence in the muon distributions at ground level gives a deep understanding of the air-showers generation in the atmosphere. Figures 8 to 12 are calculated by CORSIKA using [F] SIBYLL & FLUKA model.

Figure 8 shows the zenith angle distribution of muons with momentum $p > 0.5$ GeV/ c at the ground level. Contributions in total flux are shown from various energy ranges for the primary particles, (a) Protons and (b) Heliums. Note that the energy intervals are not the same but increase with energy. The energy bins are normalized as described in section 3. The lower zenith angles get more contribution from the lower energies of primary particles while the higher angles get more contribution from the higher energies of primary particles.

The bulk contribution from Helium contributes to higher energy bin as compared to that for proton.

Figure 9 shows the vertical muon flux as a function of momentum at the ground level for muon momentum $p > 0.5 \text{ GeV}/c$. Contributions in the total flux from various energy ranges are shown for the primary particles, (a) Protons and (b) Heliums. Note that the energy intervals are not the same but increase with energy but they are normalized as per the power law distribution. Contribution to lower energy of muons distribution comes from lower energy part of primary particles. The higher energy part of primary particles give contribution to the higher energy part of the muon distribution and thus there is a crossover between distributions of two successive energy histograms of primaries.

Figure 10 shows the muon flux distribution as a function of momentum for $p > 0.5 \text{ GeV}/c$ at 75° zenith angle. Contributions in the total flux from various energy ranges are shown for the primary particles, (a) Protons and (b) Heliums. One can notice that the contribution from higher energy bins [100-500] GeV is more dominant as compared to the lower energy bins. It shows that the muons at higher zenith angles get contributions from higher energy primary particles. One can compare it with Figure 9, where the lower energy bins were more dominating in the lower energy part of muon distribution.

Figure 11 shows the charge ratio μ^+/μ^- as a function of the momentum of atmospheric muons at the ground level calculated by CORSIKA separately for (a) Proton and (b) Helium using hadronic interaction model [F] combinations along with the experimental data collection [3]. The original references of experimental data are BESS [51], CMS [54], MINOS [55], OPERA [56] and L3+C [57]. The weight of Helium in the spectra is less than 10%. The figure shows that charge ratio would decrease with the increase in Z of the primary particles. But due to the decreasing flux of higher Z particles their weight to the spectra of charge ratio will be very small.

Figure 12 shows the multiplicity variation of muons above momentum $p > 0.5 \text{ GeV}/c$ from various energy ranges of the primary particles, (a) Protons and (b) Heliums. Each energy interval corresponds to 0.1 million events of primaries. The lower multiplicity muon events are coming mainly from the lower energy primaries and higher multiplicity events are coming from the higher energy primaries. Helium contributes more towards higher multiplicity. This study is useful to correlate the muon multiplicity at the ground with the primary particle energy.

Figure 13 shows the muon flux distributions at ground level for muon momentum $p > 0.5 \text{ GeV}/c$. The contribution of primary particles from different angle intervals are shown in (a) Zenith angle distribution of muons and (b) Momentum distribution of muons. It is clear from Figure 13(a) that the secondary particles (muons in this case) keep the memory of the direction of the primary particles and Figure 13(b) shows that the contribution to the lower energy part of the muon distributions comes from primary particles which are at lower zenith angles. The lower momentum muon flux gets more contributions from primary zenith angle between 10 to 20 degrees as compared to 0 to 10 degrees which shows the increase in the muon production with the higher path-lengths in the atmosphere. As the shower zenith angles increases further the muon survival probability also decreases. The higher momentum muons get contribution mainly from higher shower zenith angles which shows the penetration of high energy primary particles and secondary pions, kaons and other hadrons deep into the atmosphere and producing high energy muons near the Earth's surface. Contribution in the lower momentum muons from $0.5 \text{ GeV}/c$ to $5 \text{ GeV}/c$ is mainly from shower angle from 0 to 30 degrees. Contribution in the muon momentum region between $10^2 \text{ GeV}/c$ to $10^3 \text{ GeV}/c$

is nearly equal from all the shower angles and the contribution in 10^3 GeV/ c to 10^4 GeV/ c region is dominantly from showers between 70 to 90 degree.

The explanations to Figure 8 to Figure 13 are easy to understand and give us a quantitative understanding of correlation between the primary particle direction and energy with muon direction and energy.

4.3 Flux and ratios of various particles

We also looked at the distributions of other particles and their contributions at ground except the electromagnetic part. Figures 14 to 18 are calculated by CORSIKA using [F] SIBYLL & FLUKA model. Figure 14 shows the flux of the dominant cosmic ray shower particles reaching at ground level for particle momentum $p > 0.5$ GeV/ c as a function of (a) zenith angle and (b) momentum of ν_μ , $\bar{\nu}_\mu$, ν_e , $\bar{\nu}_e$, μ^+ , μ^- , n and p . The figure in (a) shows that although the muon flux falls with increasing angle, the neutrino flux remains flat and then increases towards higher angles. Neutrons and protons remain the third dominant component at the ground after neutrinos and muons. The results of Fig. 14(a) can be analyzed as follows: The muon neutrinos are produced in the production as well as in the decay of muons while the electron neutrinos are only produced in the decay of muons giving nearly twice muon neutrinos over the electron neutrinos. More muons are produced and decay at the higher zenith angles giving more and more neutrinos at the higher zenith angles. Muon flux at higher zenith angles is lower because of muon decay. Proton distribution is below neutron as they lose energy during propagation in the atmosphere. Similarly, the results of Fig. 14(b) can be analyzed as follows: The flux of muon-neutrinos in the low momentum region from 0.5 GeV/ c to 5 GeV/ c are nearly twice of the electron neutrino while towards the higher momentum side this ratio increases up to 10 to 20 times because higher momentum muons do not decay to electron neutrinos. Proton flux at higher momentum is similar to the neutron flux but there is significant difference in the lower momentum side due to the proton energy loss during its propagation in the atmosphere.

Figure 15 shows the flux of the various particles as a function of the zenith angle from the cosmic ray shower reaching at ground level for particle momentum $p > 0.5$ GeV/ c : (a) μ^+ , μ^- , π^+ , π^- , K^+ , K^- and K_L^0 and (b) $\mu^+ + \mu^-$, n , p , \bar{p} and \bar{n} . These distributions are important and if compared with the measurements will help in validation of models. After muons and nucleons, pions are the most abundant particles at the ground level.

Table 6 shows the integrated particle flux from zenith angle distribution at ground level for particle momentum $p > 0.5$ GeV/ c .

Figure 16 show the ratio of numbers of various leptons at ground level for momentum $p > 0.5$ GeV/ c as (a) zenith angle distribution and (b) momentum distribution. The $\nu_\mu/\bar{\nu}_\mu$ ratio remains flat over angle. The ratio $\nu_e/\bar{\nu}_e$ is similar to the ratio μ^+/μ^- . The ratio $(\nu_\mu + \bar{\nu}_\mu)/(\nu_e + \bar{\nu}_e)$ decreases with increasing zenith angle since muons at higher zenith angles have more probability to decay giving more number of electron neutrinos.

The measurement of ratio μ^+/μ^- can be connected to the neutrino ratios in both the flavours (e and μ) as we explain in the following. The decay of positive and negative particles (which depends on the energy and height) are given by

$$\begin{aligned} \pi^+ &\rightarrow \mu^+ + \nu_\mu \text{ and } \mu^+ \rightarrow e^+ + \bar{\nu}_\mu + \nu_e, \\ \pi^- &\rightarrow \mu^- + \bar{\nu}_\mu \text{ and } \mu^- \rightarrow e^- + \nu_\mu + \bar{\nu}_e. \end{aligned}$$

The charge ratio of survived muons at ground level will be equal to the charge ratio of

Table 6. Integrated particles flux obtained from zenith angle distribution at ground level for particle momentum $p > 0.5$ GeV/ c .

Particles (at G.L)	Area of θ distribution ($\text{m}^{-2}\text{sec}^{-1}$)	Particles (at G.L)	Area of θ distribution ($\text{m}^{-2}\text{sec}^{-1}$)
ν_μ	1657.97	π^+	0.0237
$\bar{\nu}_\mu$	1590.28	π^-	0.0178
ν_e	802.83	\bar{p}	0.0040
$\bar{\nu}_e$	679.52	\bar{n}	0.0034
μ^+	106.12	K^+	0.0001
μ^-	85.07	K^-	0.0001
n	6.07	K_L^0	0.0012
p	2.26	K_S^0	8.2244×10^{-7}

decayed muons and hence would also be equal to $\nu_e/\bar{\nu}_e$. Deviations of $\nu_e/\bar{\nu}_e$ from the muon charge ratio at ground level would require further understanding of phenomenological models and experimental data for the bulk of the air showers at ground level. Muon charge ratio is equal in the survived and total samples. At ground level, deviations of $\nu_\mu/\bar{\nu}_\mu$ from the muon charge ratio mainly comes from the opposite contributions in muon neutrinos from muon decays. Now assume if there are more μ^+ than μ^- detected at ground level and if muon survival probability was more (the case of lower zenith angle and higher momentum muons) then there will be more associated production of ν_μ than $\bar{\nu}_\mu$. In the case of higher zenith angle and lower momentum muons, the decay probability increases and hence there will be more ν_e than $\bar{\nu}_e$ and $\bar{\nu}_\mu$ than ν_μ .

Figure 17 shows the ratio of numbers of various leptons at ground level for momentum $p > 0.5$ GeV/ c as a function of zenith angle. The numerator $\nu_\mu + \bar{\nu}_\mu$ are produced in both the muon production and decay while $\nu_e + \bar{\nu}_e$ are produced only in the muon decays. The ratio $(\nu_\mu + \bar{\nu}_\mu)/(\nu_e + \bar{\nu}_e)$ gives the estimation of muon decays and hence decreases with increasing zenith angle and increases with increasing energy.

Figure 18 shows the East-west asymmetry at ground level for particle momentum $p > 0.5$ GeV/ c for (a) Neutrinos (ν_μ , $\bar{\nu}_\mu$, ν_e and $\bar{\nu}_e$) and (b) Muons (μ^+ and μ^-). Asymmetry is visible in figure (a) of neutrinos at higher zenith angles while it is not clearly seen in the case of figure (b) of muons. At the ground, more particles will reach from the west as compared to east direction because the shower of the secondary particles follows the direction of the primary cosmic particles (proton and alpha etc). These primaries are positively charged and hence are deflected by Earth's magnetic field in the west direction. It can be readily seen that east-west asymmetry is visible at higher zenith angles of the neutrinos and not visible for the muons as they lose energies in the atmosphere during propagation. Asymmetry increase at higher altitude and decrease with increasing latitude. It also depends on momentum cut on the particles.

5 Conclusions

We presented a comprehensive study of air shower simulations using various combinations of hadronic models in the CORSIKA package. Six model combinations are used one from the low energy models GHEISHA, UrQMD and FLUKA and one from the high-energy models

QGSJET, QGSJET-II and SIBYLL. In this study, we focus on the bulk of the particles at ground level and obtain the absolute yields using normalized simulation results. We have used data for muon distributions namely, zenith angle distribution, momentum distributions (at 0° and 75°) and muon charge ratios and recent parametrizations to compare with six model combinations. These distributions from various models are quantified using the χ^2 method and integrated flux obtained from all the distributions are compared among the models. All the model combinations produce the experimental shape of zenith angle distribution and underestimate the flux at very high zenith angles. Overall, GHEISHA and FLUKA give the best results for zenith angle distribution. All model combinations give a good description of momentum distribution although in the low energy region, they underestimate the flux. Overall the model combinations, UrQMD & SIBYLL and FLUKA & SIBYLL give best results. The charge ratio of muons as a function of the momentum is obtained with the different hadronic models and compared with the experimental data. The combination of models FLUKA & SIBYLL gives the best results for the muon charge ratio in the given momentum range as compared to other model combinations. The zenith angle dependence of the charge ratio of muons is predicted and compared among different models. The multiplicity distributions from different models have been obtained. The differences in the results among various models have been outlined.

Contribution in the different muon observables coming from different energies as well as zenith angle intervals of primary protons and heliums is obtained. Higher zenith angle gets more contribution from higher energies of primary particles. The muons at ground keep the memory of the direction of the primary particles.

We predict the zenith angle and momentum distribution of all other particles $\nu_\mu, \bar{\nu}_\mu, \nu_e, \bar{\nu}_e, \mu^+, \mu^-, n, p, \pi$ and K and their ratios which could be measurable at ground in addition to muons. Neutrons and protons remain the third dominant component at the ground after neutrinos and muons. These distributions are important and if compared with the measurements will lead to the validation of models. Various leptonic ratios are obtained as a function of zenith angle and momentum. These are important for a quantitative understanding of fluxes of muons and neutrino flavours and their correlations which is an important prerequisite for neutrino oscillation physics. Distribution of muons and neutrinos as a function of θ and ϕ are presented to quantify East-west asymmetry.

Acknowledgements

The authors acknowledge fruitful discussions and help in simulations from Dr. Vineet Kumar, Mr. Raman Sehgal and Sundaresh Sankrith.

References

- [1] P. K. F. Grieder, Cosmic rays at earth: Researcher's reference manual and data book, Elsevier (2001).
- [2] H. Sogarwal and P. Shukla, JCAP **07** 11, (2022).
- [3] R. L. Workman *et al.* [Particle Data Group], PTEP **083C01** (2022).
- [4] H. P. Dembinski, R. Ulrich and T. Pierog, "Future Proton-Oxygen Beam Collisions at the LHC for Air Shower Physics", PoS **ICRC2019**, 235 (2020).
- [5] D. Heck, G. Schatz, T. Thouw, J. Knapp, J. N. Capdevielle, CORSIKA: A Monte Carlo code to simulate extensive air showers, **FZKA-6019** (1998).

- [6] D. Heck, T. Pierog, Extensive air shower simulation with CORSIKA: A users guide (Version 7.7100) (2016).
- [7] N. N. Kalmykov, and S. S. Ostapchenko Phys. Atom. Nucl., 56, 346. Yad. Fiz. 56N3 (1993).
- [8] N. N. Kalmykov, S. S. Ostapchenko and A. I. Pavlov, (1994), Bull. Russ. Acad. Sci. Phys., 58, (1966).
- [9] N. N. Kalmykov, S. S. Ostapchenko and A. I. Pavlov, Nucl. Phys. Proc. Suppl., **52**, 17 (1997).
- [10] S. Ostapchenko, Phys. Rev. D **83**, 014018 (2011).
- [11] S. Ostapchenko, Phys. Rev. D **89**, 074009 (2014).
- [12] R. S. Fletcher, T. K. Gaisser, P. Lipari, and T. Stanev, Phys. Rev. D **50**, 5710 (1994).
- [13] J. Engel, T. K. Gaisser, T. Stanev and P. Lipari, 1992, Phys. Rev. D **46**, 5013 (1992).
- [14] Ahn, Eun-Joo, R. Engel, T. K. Gaisser, P. Lipari and T. Stanev, Phys. Rev. D **80**, 094003 (2009).
- [15] F. Riehn, R. Engel, A. Fedynitch, T. K. Gaisser and T. Stanev, PoS, **ICRC2015**, 558 (2016).
- [16] F. Riehn, Hadronic multiparticle production with Sibyll, KIT, Karlsruhe, Dept. Phys. <https://publikationen.bibliothek.kit.edu/1000052699> (2015).
- [17] H. Fesefeldt, The simulation of hadronic showers: Physics and Applications, PITHA-85-02 (1985).
- [18] S. A. Bass, *et. al*, Prog. Part. Nucl. Phys., **41**, 255 (1998).
- [19] M. Bleicher, *et. al*, J. Phys. G **25**, 1859 (1999).
- [20] T. T. Böhlen, F. Cerutti, M. P. W. Chin, A. Fassò, A. Ferrari, P. G. Ortega, A. Mairani, P. R. Sala, G. Smirnov and V. Vlachoudis, Nucl. Data Sheets **120**, 211 (2014).
- [21] A. Ferrari, P. R. Sala, A. Fasso and J. Ranft, **CERN-2005-10**, (2005).
- [22] T. Wibig, Chin. Phys. C **45**, 085001 (2021).
- [23] R. Engel, D. Heck, T. Huege, T. Pierog, M. Reininghaus, F. Riehn, R. Ulrich, M. Unger and D. Veberič, Comput. Softw. Big Sci. **3** no.1,2 (2019).
- [24] A. S. Barber, D. B. Kieda, Springer, R. W., Proceedings, 35th International Cosmic Ray Conference **ICRC2017**, (2017).
- [25] S. Mueller and M. Roth, PoS, **ICRC2015**, 419 (2016).
- [26] J. Wentz, I. M. Brancus, A. Bercuci, D. Heck, J. Oehlschlager, H. Rebel and B. Vulpesu, Phys. Rev. D **67**, 073020, (2003).
- [27] T. Djemil, R. Attallah and J. N. Capdevielle, Int. J. Mod. Phys. A **20** 6950 (2005).
- [28] R. V. Nikolaenko, A. G. Bogdanov, R. P. Kokoulin and A. A. Petrukhin, Phys. At. Nucl. **84**, 1011 (2021).
- [29] S. M. H. Halataei, M. Bahmanabadi, M. K. Ghomi and J. Samimi, Phys. Rev. D **77**, 083001 (2008).
- [30] P. Patgiri, D. Kalita and K. Boruah, Indian J. Phys. **91**, 351 (2017).
- [31] M. Bahmanabadi and L. Rafezi, Phys. Rev. D **98**, 103003 (2018).
- [32] M. Bahmanabadi, Nucl. Instrum. Meth. A **945**, 162635 (2019).
- [33] M. Bahmanabadi and M. Fazlalizadeh, Phys. Rev. D **100**, 083004 (2019).
- [34] A. Cohu, M. Tramontini, A. Chevalier, J. Marteau and J. C. Ianigro, JAIS **2022**, 250 (2022).
- [35] P. Shukla and S. Sankrith, Int. J. Mod. Phys. A **33**, 1850175 (2018).

- [36] Gaisser, T. K., *Astropart. Phys.*, **16**, 285 (2002).
- [37] K. Abe, *et. al*, *Astrophys. J.* **822**, 65 (2016).
- [38] O. Adriani et al. (PAMELA), *Science* **332**, 69 (2011).
- [39] M. Aguilar et al. (AMS), *Phys. Rev. Lett.* **114**, 171103 (2015).
- [40] K. Asakimori et al., *Astrophys. J.* **502**, 278 (1998).
- [41] A.D. Panov et al. (ATIC Collab.), *Bull. Russian Acad. of Science, Physics*, **73**, 564 (2009).
- [42] V.A. Derbina, *et. al* (RUNJOB), *Astrophys. J.* **628**, L41 (2005).
- [43] M. Aguilar et al. (AMS), *Phys. Rev. Lett.* **115**, 211101 (2015).
- [44] T. Pierog *et al.*, *Phys. Rev. C* **92**, 034906 (2015).
- [45] G. Graziani, *PoS, ICRC2017*, 214 (2017).
- [46] S. Cecchini, and M. Spurio, 2012, arXiv:1208.1171 (astro-ph).
- [47] J. N. Crookes, and B. C. Rastin, *Nucl. Phys. B* **39**, 493 (1972).
- [48] A. N. Dmitrieva, *et. al*, *Phys. Atom. Nucl.* **69**, 865 (2006).
- [49] R. W. Flint, and R. B. Hicks, and S. Standil *Can. J. Phys.* **50**, 843 (1972).
- [50] M. Gettert, and J. Unger and R. Trezeciak, and J. Engler and J. Knapp, *Proc. 23rd International Cosmic Ray Conference (ICRC)*, Calgary, 4, 394 (1993).
- [51] Haino, S. *et. al*, *Phys. Lett. B* **594**, 35 (2004).
- [52] B. C. Rastin, *J. Phys. G* **10**, 1609 (1984).
- [53] H. Jokisch, K. Carstensen, W. D. Dau, H. J. Meyer and O. C. Allkofer, *Phys. Rev. D* **19**, 1368 (1979).
- [54] V. Khachatryan *et al.* [CMS], *Phys. Lett. B* **692**, 83 (2010).
- [55] P. Adamson *et al.* [MINOS], *Phys. Rev. D* **76**, 052003 (2007).
- [56] N. Agafonova *et al.* [OPERA], *Eur. Phys. J. C* **67**, 25 (2010).
- [57] P. Achard *et al.* [L3], *Phys. Lett. B* **598**, 15 (2004).

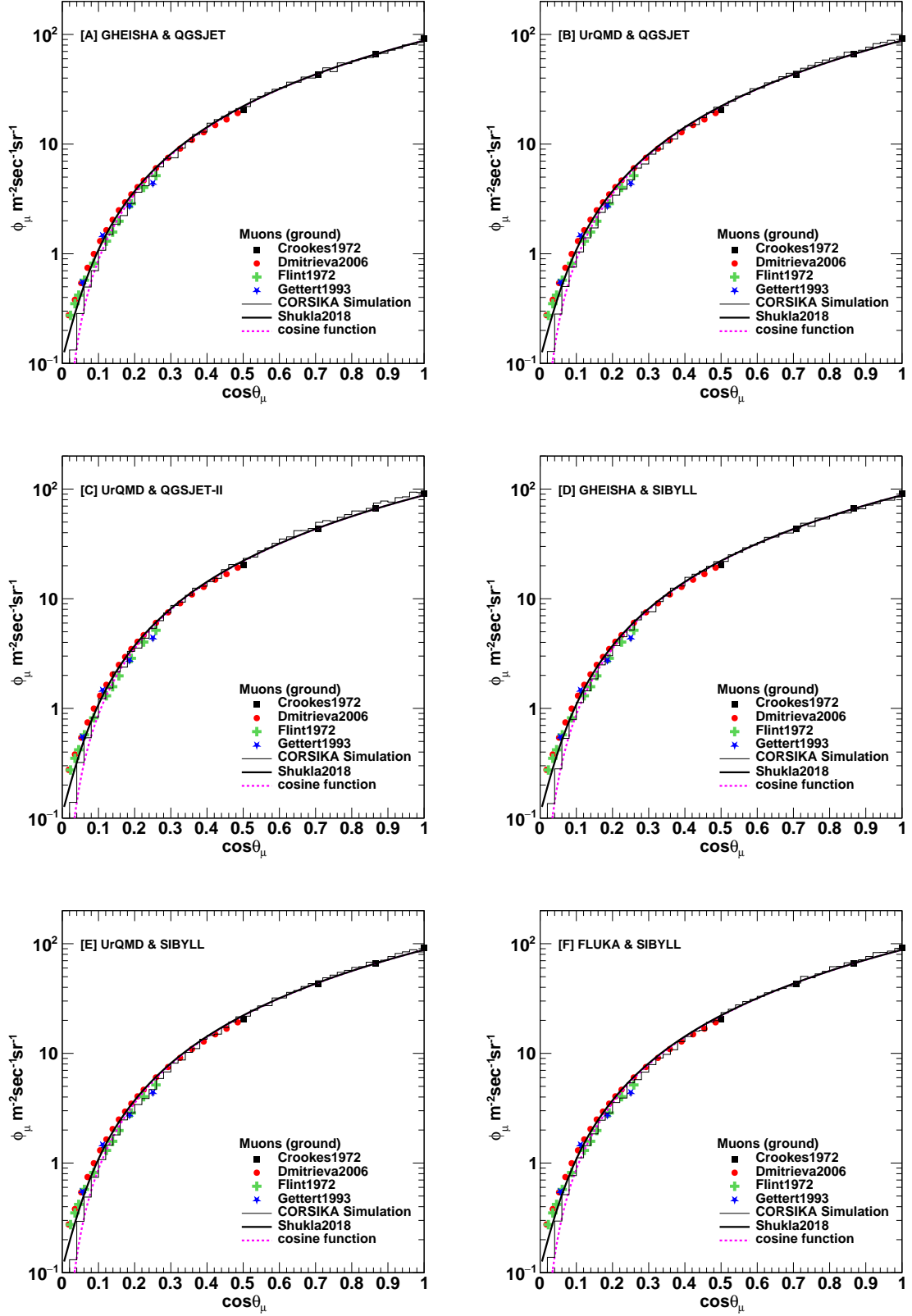


Figure 2. The zenith angle distributions calculated from CORSIKA using various model combinations for muon momentum $p > 0.5$ GeV/c along with data measured by various experiments. The parameterization is given by Eq. 2.2 is also shown [35]. The data are taken from the collection of Ref. [46].

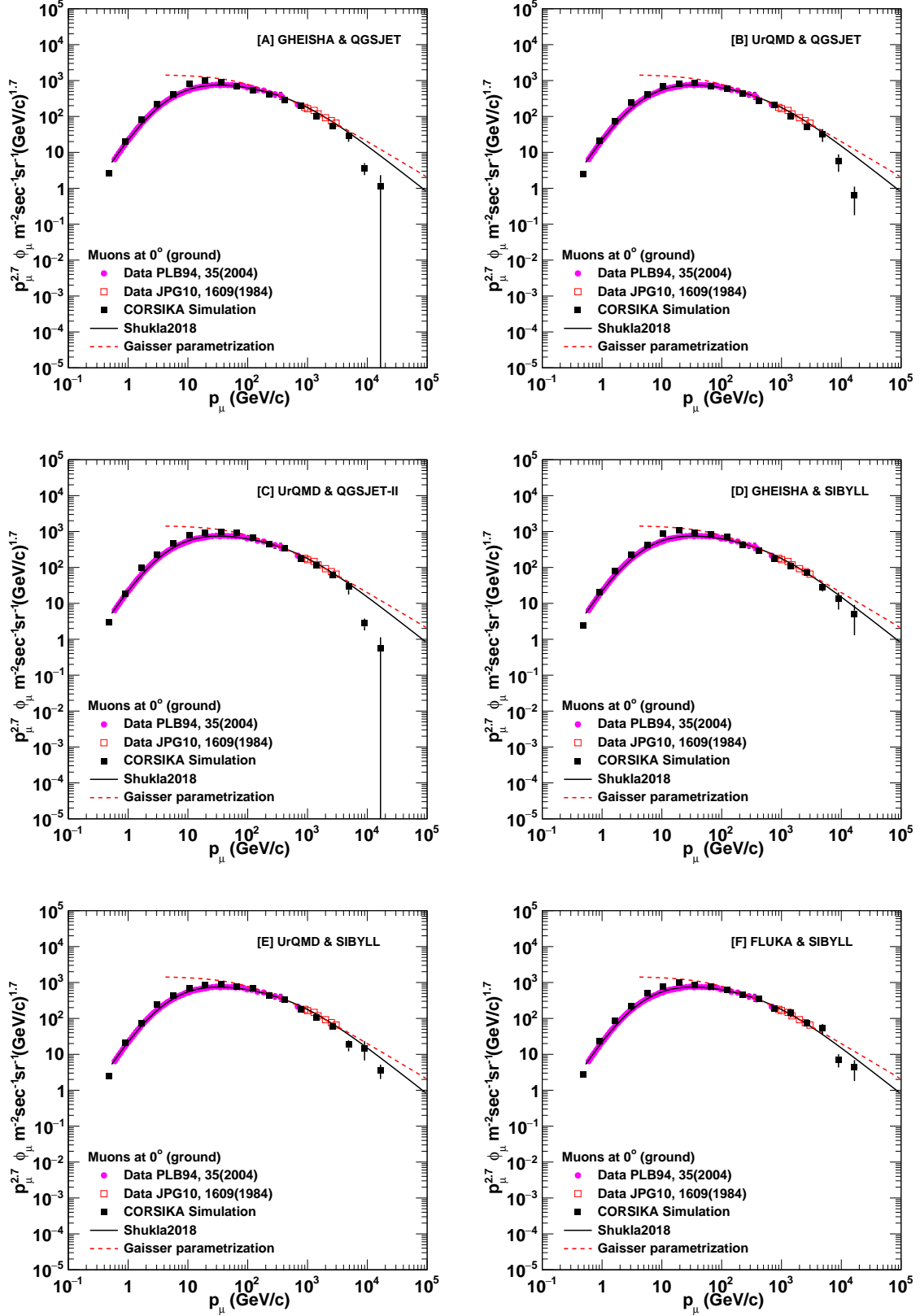


Figure 3. The momentum distribution of vertical atmospheric muons at the ground level calculated by CORSIKA using different hadronic interaction model combinations for muon momentum $p > 0.5$ GeV/c along with the experimental data [51, 52]. The parametrizations given by Eq.2.1 [35] and Eq.2.5 [36] are also shown.

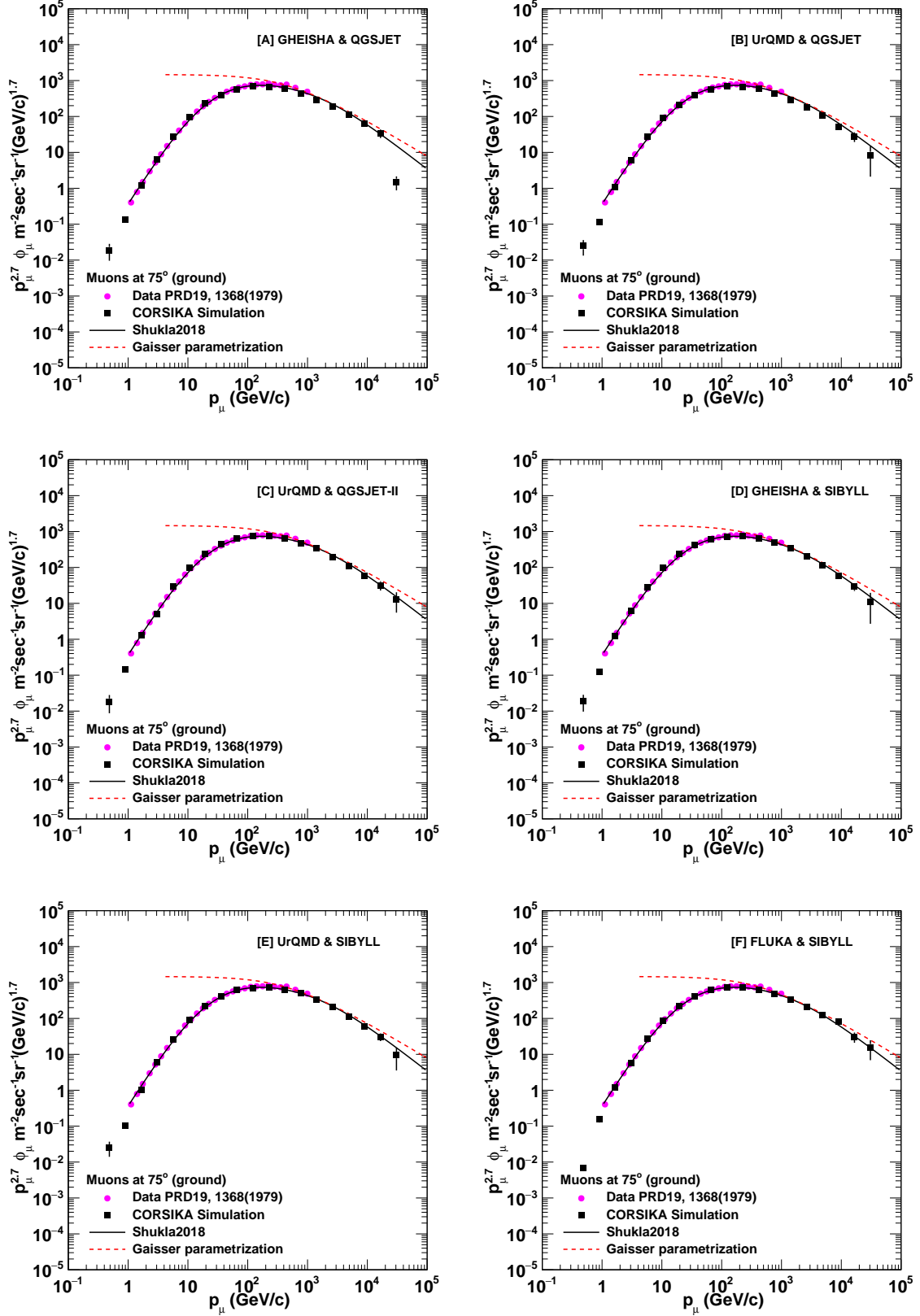


Figure 4. The momentum distribution of atmospheric muons at 75° zenith angle at the ground level calculated by CORSIKA using different hadronic interaction model combinations for $p > 0.5$ GeV/c along with the experimental data [53]. The parametrizations given by Eq. 2.1 and Eq. 2.5 are also shown.

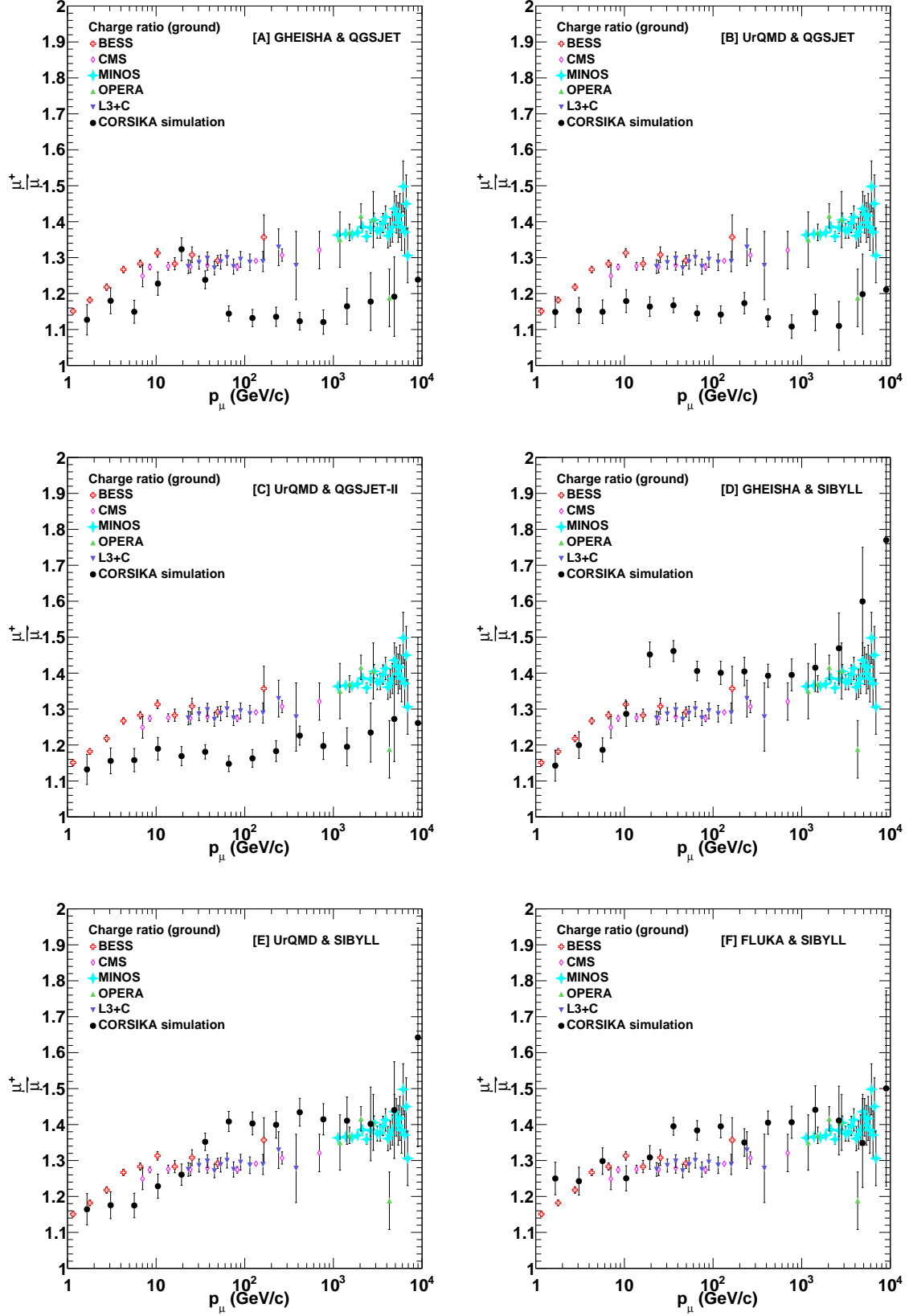


Figure 5. The charge ratio μ^+/μ^- as a function of momentum of atmospheric muons at the ground level calculated by CORSIKA using different hadronic interaction model combinations along with the experimental data collection [3].

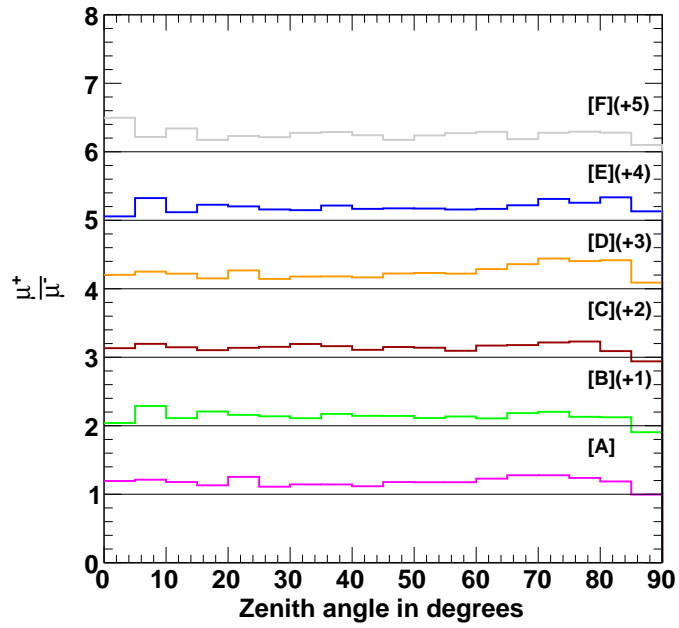


Figure 6. The charge ratio μ^+/μ^- as a function of zenith angle of atmospheric muons for momentum $p > 0.5$ GeV/ c at the ground level calculated by CORSIKA using different hadronic interaction model combinations, [A] GHEISHA & QGSJET, [B] UrQMD & QGSJET, [C] UrQMD & QGSJET-II, [D] GHEISHA & SIBYLL, [E] UrQMD & SIBYLL, [F] FLUKA & SIBYLL. Integer numbers are added to models other than [A] as shown to separate the results.

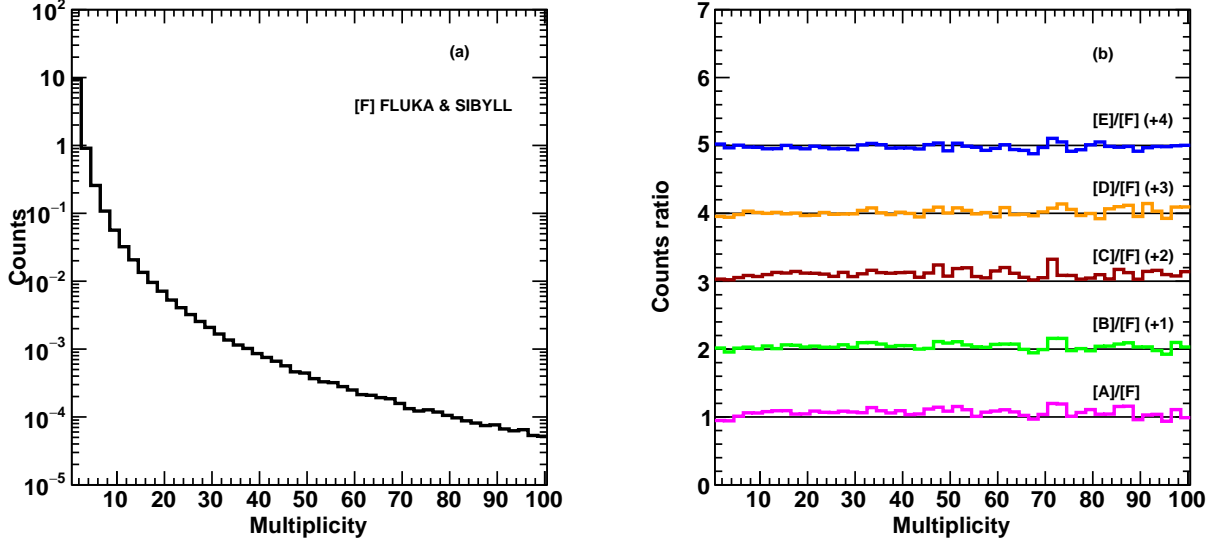


Figure 7. The multiplicity of muon in a shower calculated for muon momentum $p > 0.5$ GeV/c using the (a) [F] FLUKA & SIBYLL models of CORSIKA. (b) Multiplicity ratio of model combinations ([A] GHEISHA & QGSJET, [B] UrQMD & QGSJET, [C] UrQMD & QGSJET-II, [D] GHEISHA & SIBYLL and [E] UrQMD & SIBYLL) with respect to [F] FLUKA & SIBYLL model. An integer number is added to each model result as shown in figure.

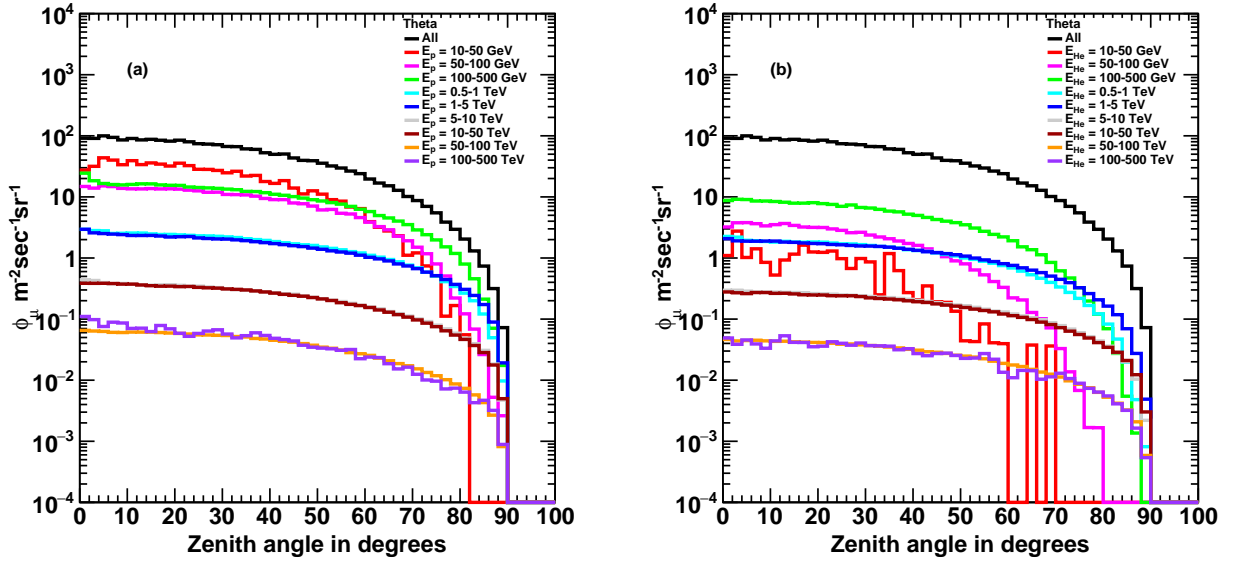


Figure 8. The zenith angle distribution of muons with momentum $p > 0.5$ GeV/c at the ground level. Contributions in total flux are shown from various energy ranges for the primary particles, (a) Protons and (b) Heliums. Note that the energy intervals are not the same but increase with energy. The relative contribution of each bin is normalized as described in section 3.

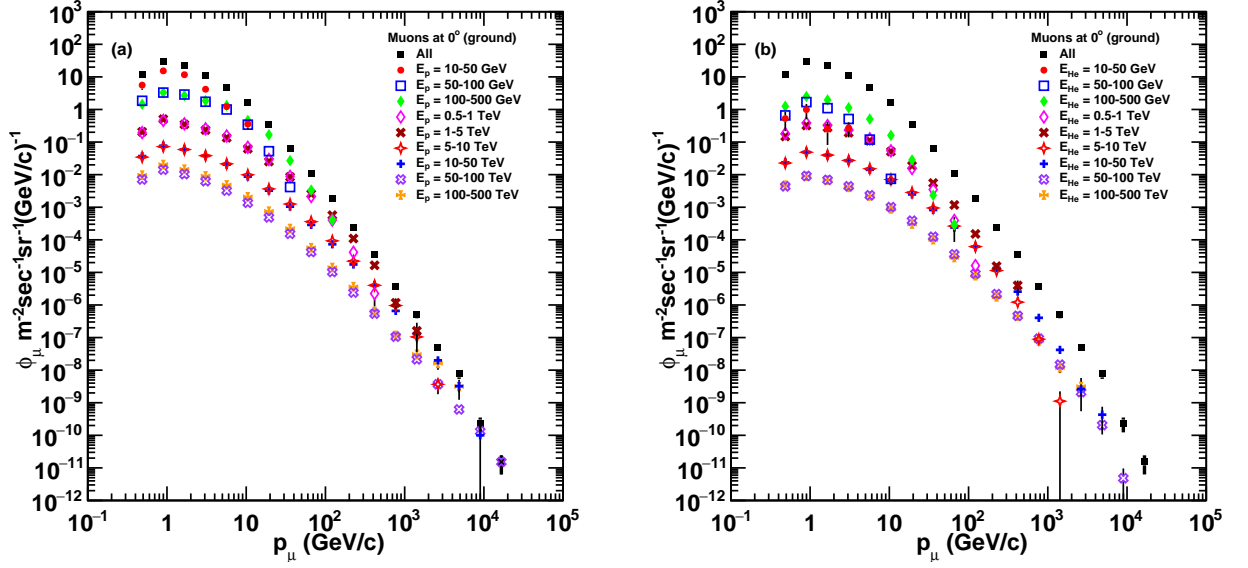


Figure 9. Vertical muon flux as a function of momentum for muon momentum $p > 0.5$ GeV/ c at the ground level. Contributions in the total flux from various energy ranges are shown for the primary particles, (a) Proton and (b) Helium.

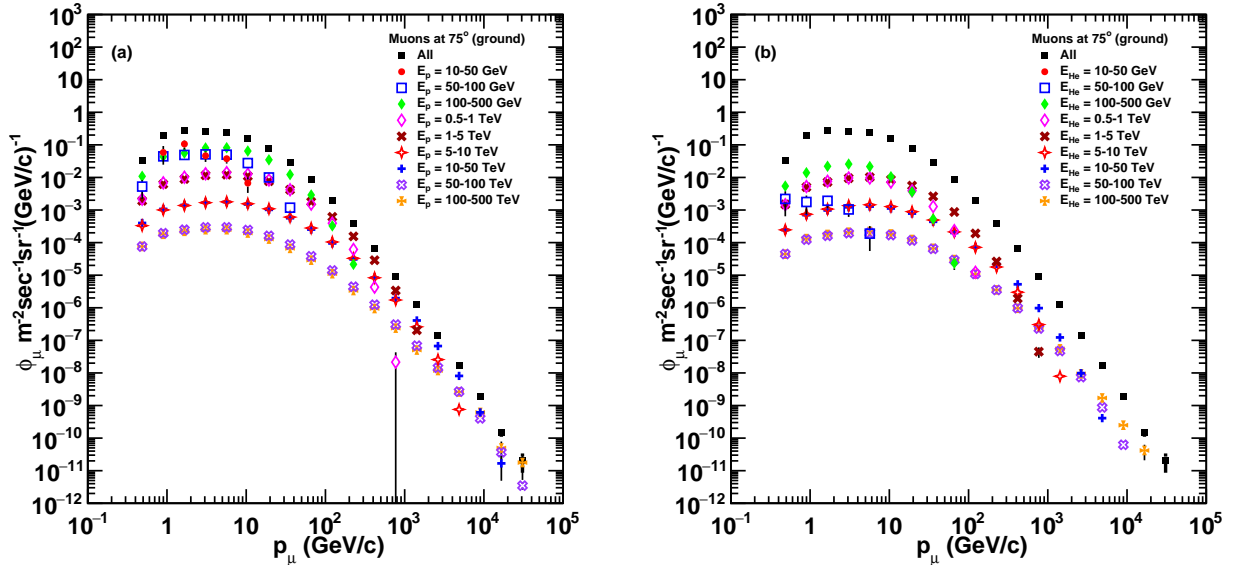


Figure 10. Muon flux distribution as a function of momentum at the ground level for $p > 0.5$ GeV/ c at 75° zenith angle. Contributions in the total flux from various energy ranges are shown for the primary particles, (a) Proton and (b) Helium.

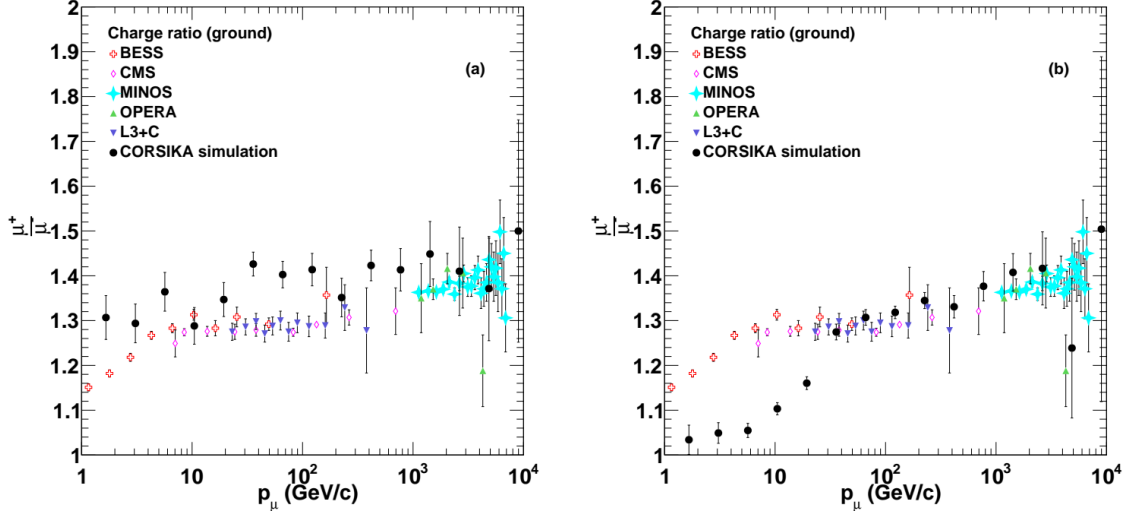


Figure 11. The charge ratio μ^+/μ^- as a function of momentum of atmospheric muons at the ground level calculated by CORSIKA for (a) Proton and (b) Helium using hadronic interaction model combinations [F] along with the experimental data collection [3].

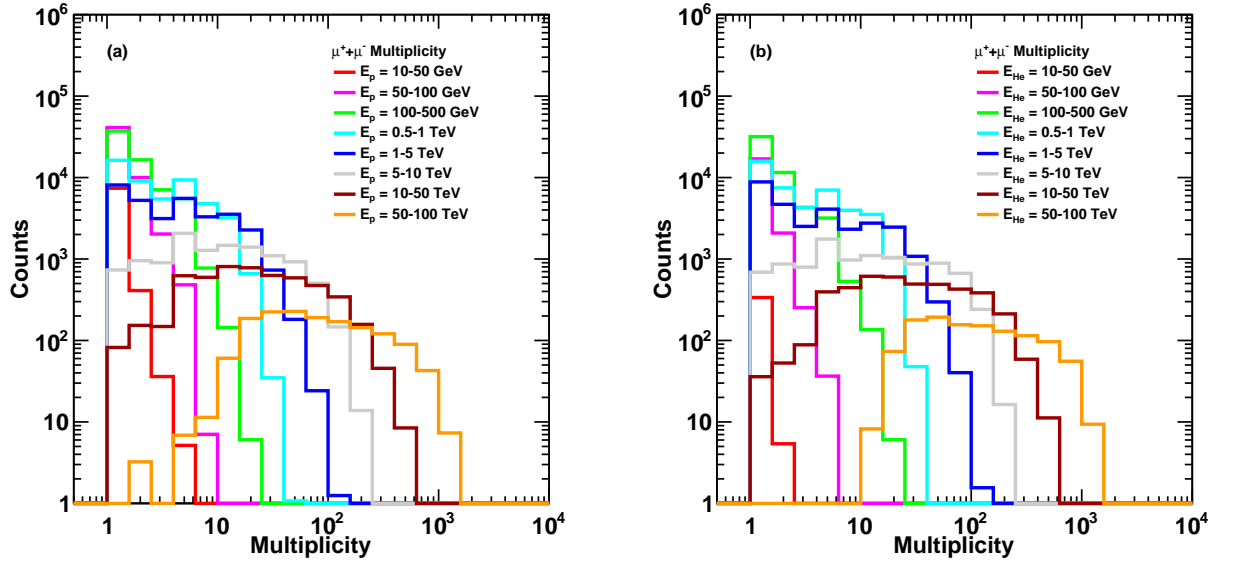


Figure 12. Multiplicity variation of cosmic muons above momentum $p > 0.5$ GeV/c from various energy ranges of the primary particles, (a) Protons and (b) Heliums. Each energy interval corresponds to 0.1 million events of primaries.

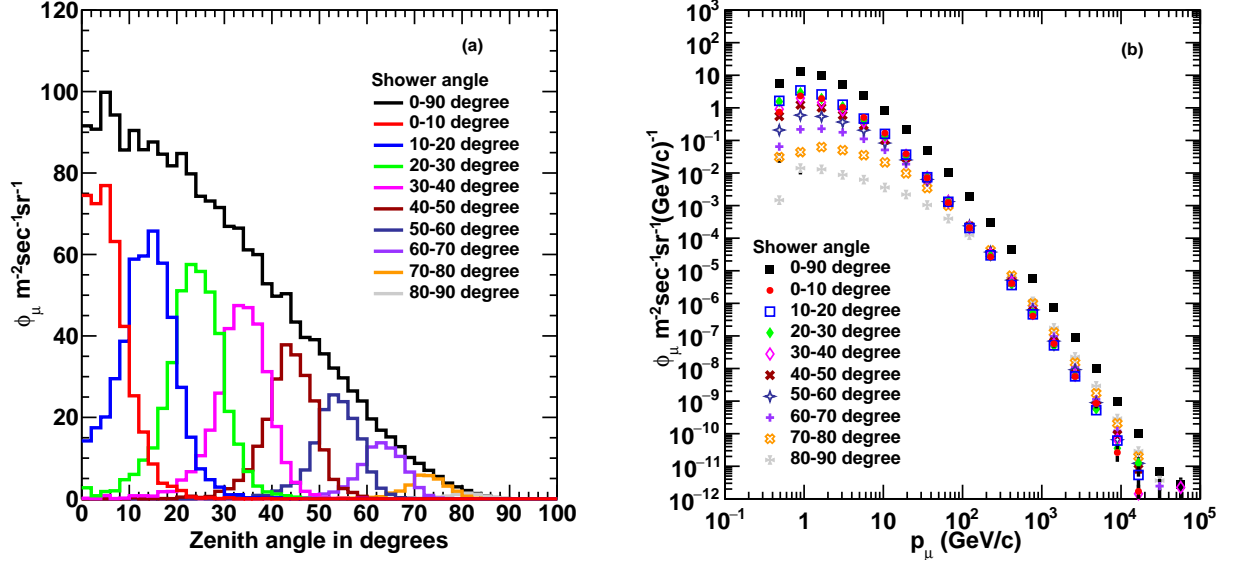


Figure 13. Muon flux distributions at ground level for muon momentum $p > 0.5 \text{ GeV}/c$. The contributions of primary particles from different angle intervals are shown in (a) Zenith angle distribution of muons and (b) Momentum distribution of muons.

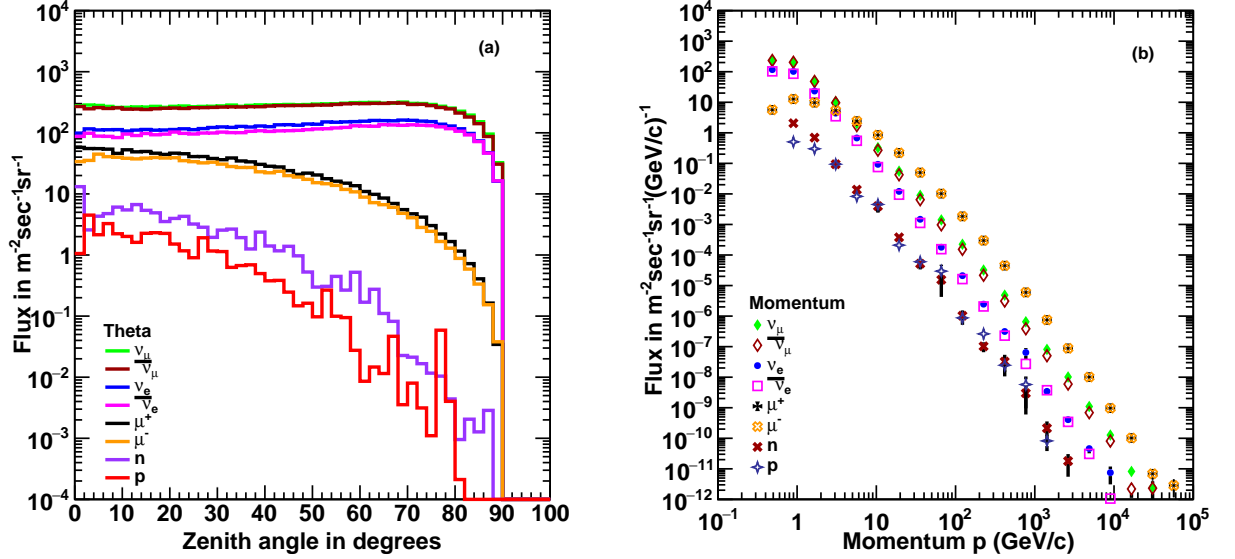


Figure 14. The flux of dominant cosmic ray shower particles reaching at ground level for particle momentum $p > 0.5 \text{ GeV}/c$ as a function of (a) Zenith angle and (b) Momentum of ν_μ , $\bar{\nu}_\mu$, ν_e , $\bar{\nu}_e$, μ^+ , μ^- , n and p .

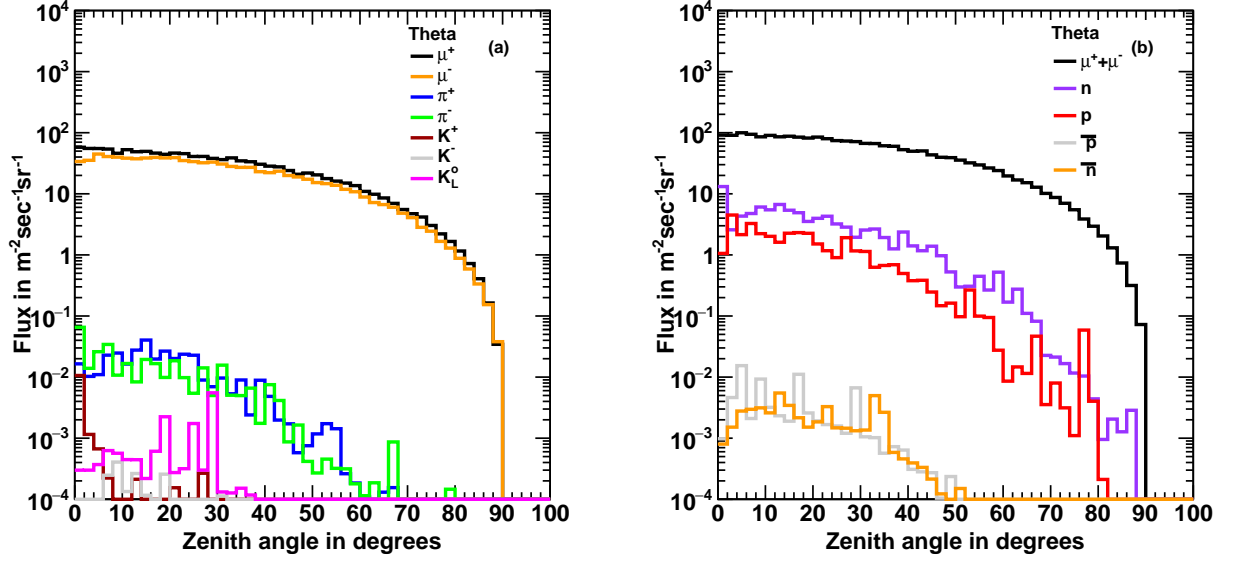


Figure 15. Flux of the various particles as a function of the zenith angle from the cosmic ray shower reaching at ground level for particle momentum $p > 0.5$ GeV/c: (a) μ^+ , μ^- , π^+ , π^- , K^+ , K^- and K_L^0 and (b) $\mu^+\mu^-$, n , p , \bar{p} and \bar{n} .

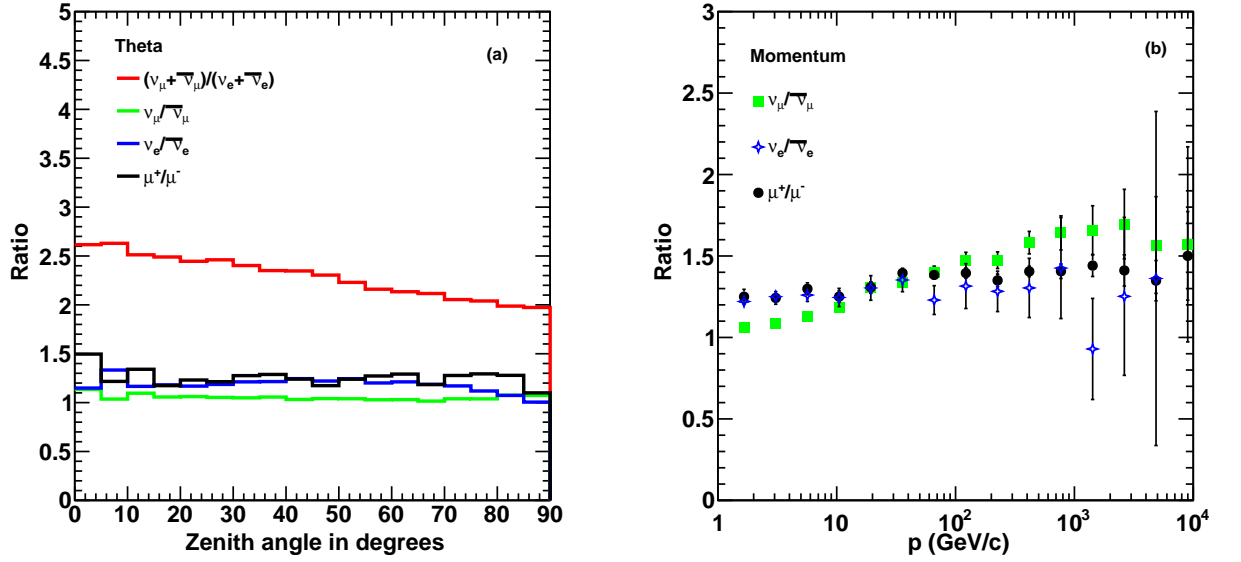


Figure 16. Ratio of various leptons for momentum $p > 0.5$ GeV/c at ground level (a) Zenith angle distribution and (b) Momentum distribution.

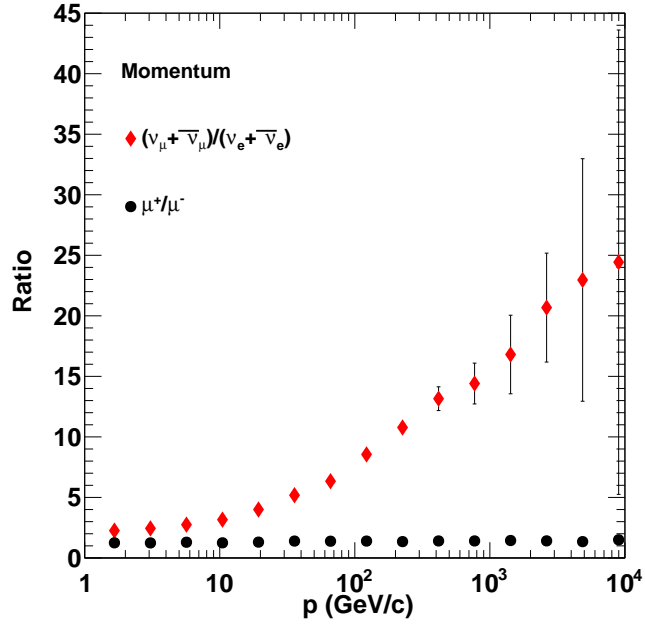


Figure 17. Ratio of numbers of various leptons for momentum $p > 0.5$ GeV/ c at ground level (a) Zenith angle distribution and (b) Momentum distribution.

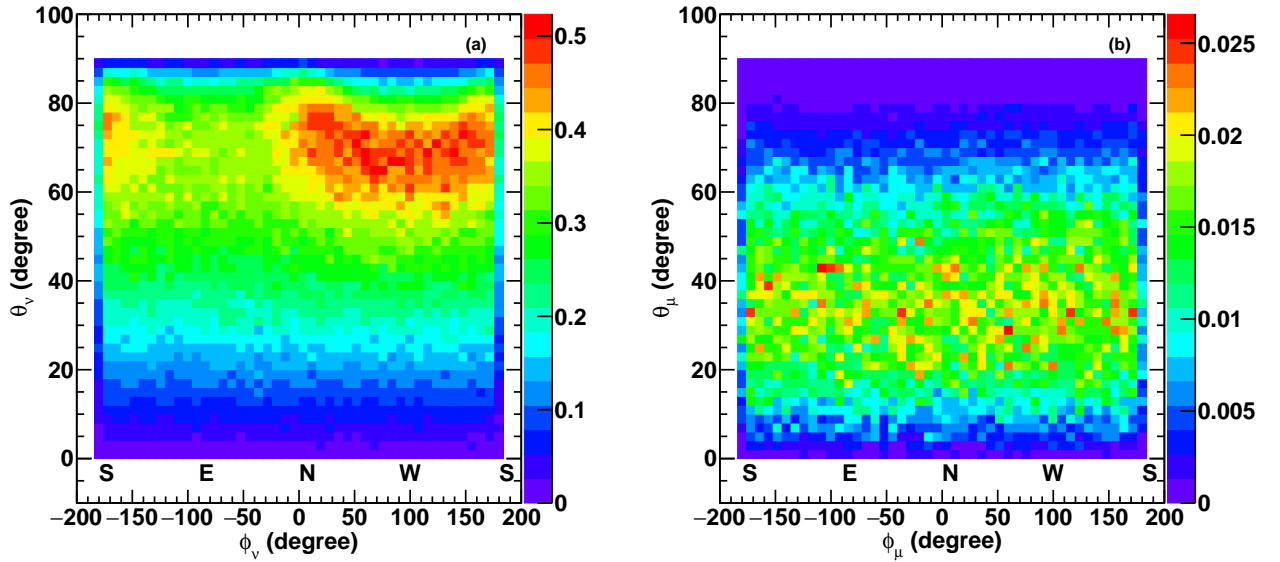


Figure 18. East-west asymmetry at ground level for particle momentum $p > 0.5$ GeV/ c for (a) Neutrinos (ν_μ , $\bar{\nu}_\mu$, ν_e and $\bar{\nu}_e$) and (b) Muons (μ^+ and μ^-).